iScience

CellPress
OPEN ACCESS

Article

Genome-wide association study of hippocampal blood-oxygen-level-dependent-cerebral blood flow correlation in Chinese Han population

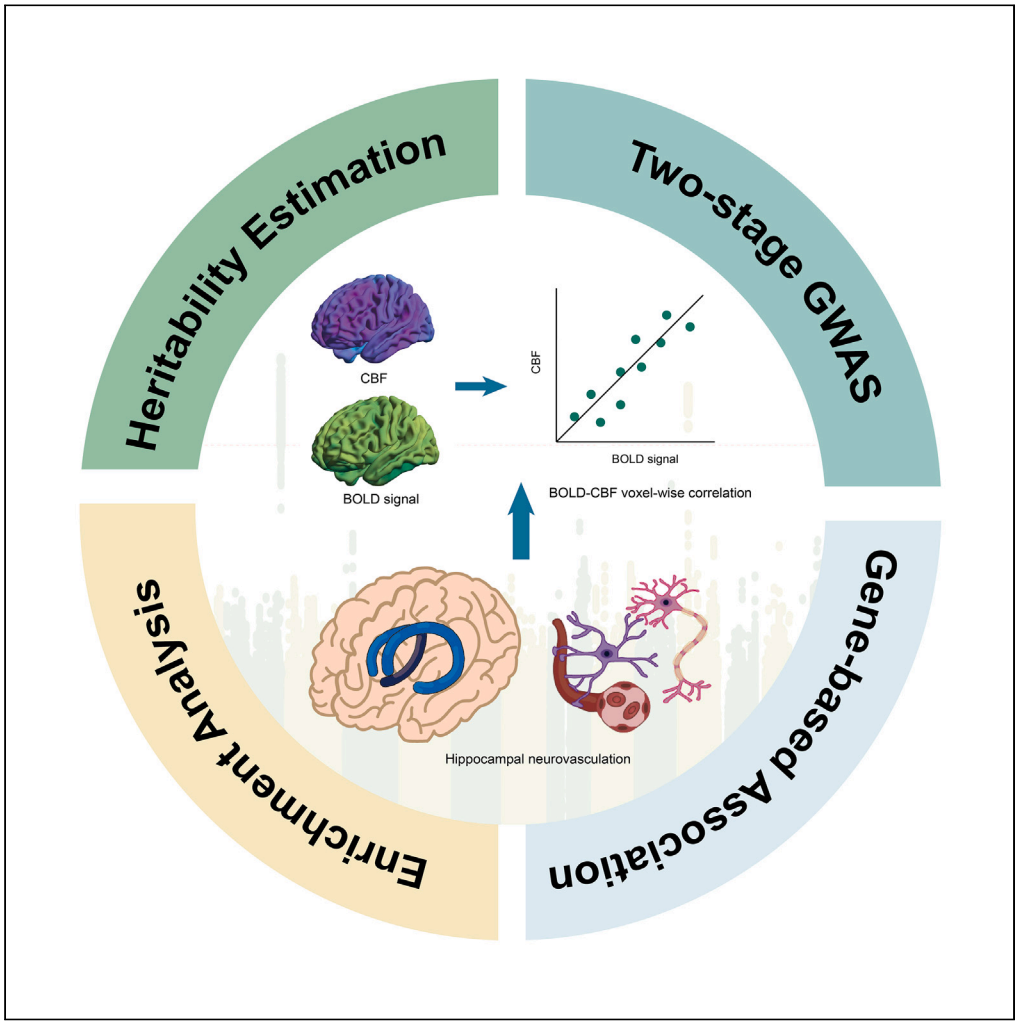

Hui Xue, Xiaojun Xu, Zhihan Yan, ..., Junfang Xian, Chunshui Yu, the CHIMGEN Consortium

yuyongqiang@ahmu.edu.cn (Y.Y.)
cjr.xianjunfang@vip.163.com (J.X.)
chunshuiyu@tmu.edu.cn (C.Y.)

Highlights

The genetic architecture of hippocampal BOLD-CBF correlation remains unknown

The heritability of hippocampal BOLD-CBF correlation was estimated 16.2–23.9%

2 independent significant loci were revealed by two-stage GWAS

Gene-based association analyses showed 4 significant genes

Xue et al., iScience 26, 108005
October 20, 2023
https://doi.org/10.1016/j.isci.2023.108005

iScience

CellPress
OPEN ACCESS

Article

Genome-wide association study of hippocampal blood-oxygen-level-dependent-cerebral blood flow correlation in Chinese Han population

Hui Xue,[1,23] Xiaojun Xu,[2,23] Zhihan Yan,[3,23] Jingliang Cheng,[4] Longjiang Zhang,[5] Wenzhen Zhu,[6] Guangbin Cui,[7] Quan Zhang,[8] Shijun Qiu,[9] Zhenwei Yao,[10] Wen Qin,[1] Feng Liu,[1] Meng Liang,[11] Jilian Fu,[1] Qiang Xu,[1] Jiayuan Xu,[1] Yingying Xie,[1] Peng Zhang,[12] Wei Li,[12] Caihong Wang,[4] Wen Shen,[13] Xiaochu Zhang,[14] Kai Xu,[15] Xi-Nian Zuo,[16,17] Zhaoxiang Ye,[18] Yongqiang Yu,[19,*] Junfang Xian,[20,*] Chunshui Yu,[1,21,24,*] and On behalf of the CHIMGEN Consortium[22]

SUMMARY

Correlation between blood-oxygen-level-dependent (BOLD) and cerebral blood flow (CBF) has been used as an index of neurovascular coupling. Hippocampal BOLD-CBF correlation is associated with neurocognition, and the reduced correlation is associated with neuropsychiatric disorders. We conducted the first genome-wide association study of the hippocampal BOLD-CBF correlation in 4,832 Chinese Han subjects. The hippocampal BOLD-CBF correlation had an estimated heritability of 16.2–23.9% and showed reliable genome-wide significant association with a locus at 3q28, in which many variants have been linked to neuroimaging and cerebrospinal fluid markers of Alzheimer's disease. Gene-based association analyses showed four significant genes (*GMNC*, *CRTC2*, *DENND4B*, and *GATAD2B*) and revealed enrichment for mast cell calcium mobilization, microglial cell proliferation, and ubiquitin-related proteolysis pathways that regulate different cellular components of the neurovascular unit. This is the first unbiased identification of the association of hippocampal BOLD-CBF correlation, providing fresh insights into the genetic architecture of hippocampal neurovascular coupling.

INTRODUCTION

About a half million of studies have applied the blood-oxygen-level-dependent (BOLD) functional magnetic resonance imaging (fMRI) to investigate brain function in healthy individuals and patients with neuropsychiatric disorders. BOLD-fMRI depends on the neurobiological mechanism of neurovascular coupling (NVC) whereby local cerebral blood flow (CBF) rapidly increases following regional neural activity.[1,2]

[1]Department of Radiology and Tianjin Key Laboratory of Functional Imaging, Tianjin Medical University General Hospital, Tianjin 300052, China
[2]Department of Radiology, The Second Affiliated Hospital of Zhejiang University, School of Medicine, Hangzhou 310009, China
[3]Department of Radiology, The Second Affiliated Hospital and Yuying Children's Hospital of Wenzhou Medical University, Wenzhou 325027, China
[4]Department of Magnetic Resonance Imaging, The First Affiliated Hospital of Zhengzhou University, Zhengzhou 450052, China
[5]Department of Radiology, Jinling Hospital, Affiliated Hospital of Medical School, Nanjing University, Nanjing 210002, China
[6]Department of Radiology, Tongji Hospital, Tongji Medical College, Huazhong University of Science and Technology, Wuhan 430030, China
[7]Functional and Molecular Imaging Key Lab of Shaanxi Province & Department of Radiology, Tangdu Hospital, Air Force Medical University, Xi'an 710038, China
[8]Department of Radiology, Characteristic Medical Center of Chinese People's Armed Police Force, Tianjin 300162, China
[9]Department of Medical Imaging, the First Affiliated Hospital of Guangzhou University of Traditional Chinese Medicine, Guangzhou 510405, China
[10]Department of Radiology, Huashan Hospital, Fudan University, Shanghai 200040, China
[11]School of Medical Imaging and Tianjin Key Laboratory of Functional Imaging, Tianjin Medical University, Tianjin 300203, China
[12]Department of Radiology, Tianjin Medical University Cancer Institute and Hospital, Tianjin 300060, China
[13]Department of Radiology, Tianjin First Center Hospital, Tianjin 300192, China
[14]Division of Life Science and Medicine, University of Science & Technology of China, Hefei 230027, China
[15]Department of Radiology, The Affiliated Hospital of Xuzhou Medical University, Xuzhou 221006, China
[16]Developmental Population Neuroscience Research Center at IDG/McGovern Institute for Brain Research, Beijing Normal University, Beijing 100875, China
[17]Institute of Psychology, Chinese Academy of Sciences, Beijing 100101, China
[18]Department of Radiology, Tianjin Medical University Cancer Institute and Hospital, National Clinical Research Center for Cancer, Tianjin's Clinical Research Center for Cancer, Tianjin Medical University, Ministry of Education, Key Laboratory of Cancer Prevention and Therapy, Tianjin 300060, China
[19]Department of Radiology, The First Affiliated Hospital of Anhui Medical University, Hefei 230022, China
[20]Department of Radiology, Beijing Tongren Hospital, Capital Medical University, Beijing 100730, China
[21]CAS Center for Excellence in Brain Science and Intelligence Technology, Chinese Academy of Sciences, Shanghai 200031, China
[22]Further details can be found in the supplemental information
[23]These authors contributed equally
[24]Lead contact
*Correspondence: yuyongqiang@ahmu.edu.cn (Y.Y.), cjr.xianjunfang@vip.163.com (J.X.), chunshuiyu@tmu.edu.cn (C.Y.)
https://doi.org/10.1016/j.isci.2023.108005

NVC depends on the concerted action of cellular components of neurovascular unit (NVU), including neurons and astrocytes from brain parenchyma, as well as pericytes, smooth muscle cells and endothelial cells from blood vessels.[3] NVC is a critical mechanism for any brain structure to maintain its normal function and neurovascular uncoupling has been associated with neuropsychiatric disorders, such as Alzheimer's disease (AD), stroke, and autism spectrum disorder.[4,5]

With *in vivo* brain magnetic resonance imaging (MRI) techniques, BOLD-CBF correlation has been used as a proxy to reflect NVC. Regional BOLD-CBF correlation varies across individuals and is correlated with age, sex, and executive function.[6] In addition, alterations in regional BOLD-CBF correlations have been observed in many neuropsychiatric disorders, such as AD,[7] schizophrenia,[8] subcortical ischemic vascular disease,[9] and generalized anxiety disorder.[10] These results indicate that BOLD-CBF correlation may be an individual trait, however, there are still lacking genome-wide association studies (GWASs) on regional BOLD-CBF correlation.

The hippocampus is critically important for human memory, navigation, and other cognitive functions,[11,12] and is implicated in common brain disorders, such as AD and schizophrenia.[13,14] A unique ability of the hippocampus is to generate new neurons throughout life and neurogenesis is regulated by the hippocampal NVC.[15] The newborn neurons can be integrated into the existing neural circuitry of cognitive control, and their dysfunction has been associated with cognitive impairments and dementia.[16] The hippocampus shows much lower NVC than neocortical regions due to microvascular differences, which could explain why the hippocampus is more vulnerable than other regions in brain disorders with reduced energy supply.[17] For instance, the hippocampal NVC reduction is considered as a potential biomarker of AD[18,19]; the peak latency of the hemodynamic response function (HRF-PL) of hippocampus is associated with stress response and risk for depression[20]; and hippocampal BOLD-CBF correlation is altered in patients with schizophrenia[6] and diabetes mellitus.[21] Considering the critical role of the hippocampal NVC, there is an urgent need to investigate the genetic architecture of the hippocampal BOLD-CBF correlation.

In this study, we conducted the first GWAS on the hippocampal BOLD-CBF correlation in 4,832 Chinese Han participants from the Chinese Imaging Genetics (CHIMGEN) cohort.[22] Here, the across-voxel correlation between reginal homogeneity (ReHo) derived from the resting-state fMRI data and CBF measured by the arterial spin labeling (ASL) MRI data within hippocampal voxels was used as a proxy to represent hippocampal NVC. The study design is illustrated in Figure S1.

RESULTS

Subjects

This study included 4,832 Chinese Han healthy young subjects with qualified genomic, resting-state fMRI, and ASL data from 17 centers of the CHIMGEN study. Since the scanner effect which was variability caused by MRI data acquired by different scanners is a major bias in multi-center neuroimaging studies causing reduced reliability of neuroimaging measurements,[23] we divided subjects into the discovery and replication samples based on the types of MRI scanners. Of the 4,832 subjects, 4,406 subjects (2,778 females; age: 23.6 $\pm$ 2.4 years) were defined as the discovery sample since their MRI data were acquired by the same type (GE Discovery MR750) of scanners with the same scanning parameters, in which the bias from the scanner effect was expected to be small. We defined other 426 subjects (283 females; age: 24.0 $\pm$ 2.4 years) whose MRI data were acquired by different types of scanners as the replication sample. The mixed replication sample can test whether the discovered results are applicable for MRI data acquired by different types of MRI scanners. The demographic data of the included subjects are shown in Table S1 and the distribution of these subjects across centers is presented in Table S2.

Hippocampal blood-oxygen-level-dependent-cerebral blood flow correlation calculation

In the main analysis, the hippocampal BOLD-CBF correlation of each subject was measured by ReHo-CBF correlation, the across-voxel correlation coefficient between ReHo and CBF, in bilateral hippocampal voxels defined by the automated anatomical atlas (AAL)[24] in the standard space. Here, ReHo was used to measure spontaneous neuronal activity and was calculated based the preprocessed fMRI data without global signal regression (GSR). The distribution of the average ReHo-CBF correlations across AAL regions are presented in Figure S2, revealing that ReHo-CBF correlation was disparate in different brain region and was consistent with previous study.[6] Since MRI data were acquired from different scanners, we used the Combat approach[25] with sex and age as covariates to alleviate the scanner effects on these brain imaging measures and found that Combat harmonization could reduce between-scanner variations of hippocampal ReHo and CBF (Figure S3). After harmonization, the age, sex, and site explained 0.038% ($\beta = -0.019$, $p = 0.18$), 1.14% ($\beta = -0.13$, $p = 1.43 \times 10^{-13}$), and 0.11% ($\beta = -0.033$, $p = 0.021$) variance of ReHo-CBF correlation, respectively. The calculation process of the hippocampal BOLD-CBF correlation is illustrated in Figure 1.

Since there is no standard pipeline to calculate the hippocampal NVC based on MRI data, we also used other four approaches to compute the measure to verify our main findings in these analyses. To test the impact of the selection of fMRI measure to represent spontaneous neuronal activity, we also used the amplitude of low-frequency fluctuation (ALFF) of BOLD signals and fractional ALFF (fALFF) to represent spontaneous neuronal activity and defined the hippocampal BOLD-CBF correlation as ALFF-CBF correlation and fALFF-CBF correlation. To test the impact of selecting brain atlas to extract the hippocampal voxels, we also extracted the hippocampal voxels from the Brainnetome atlas (BNA)[26] and recalculated the hippocampal ReHo-CBF correlation. To test the impact of GSR during the fMRI data preprocessing, we regressed out global BOLD signals and recalculated ReHo-CBF correlation (ReHo-CBF-GSR). The hippocampal BOLD-CBF correlations estimated by the five methods were highly correlated (r values ranged from 0.84 to 0.98) (Figure S4). We also tested the intra-class correlation coefficients (ICC) of these measures based on MRI data from eight participants who received MR scans at two different time points. We found that the ICC was 0.914 ($p = 0.015$), 0.986 ($p = 0.0029$), and 0.973 ($p = 0.007$) for the ReHo-CBF, ALFF-CBF, and fALFF-CBF correlations, respectively.

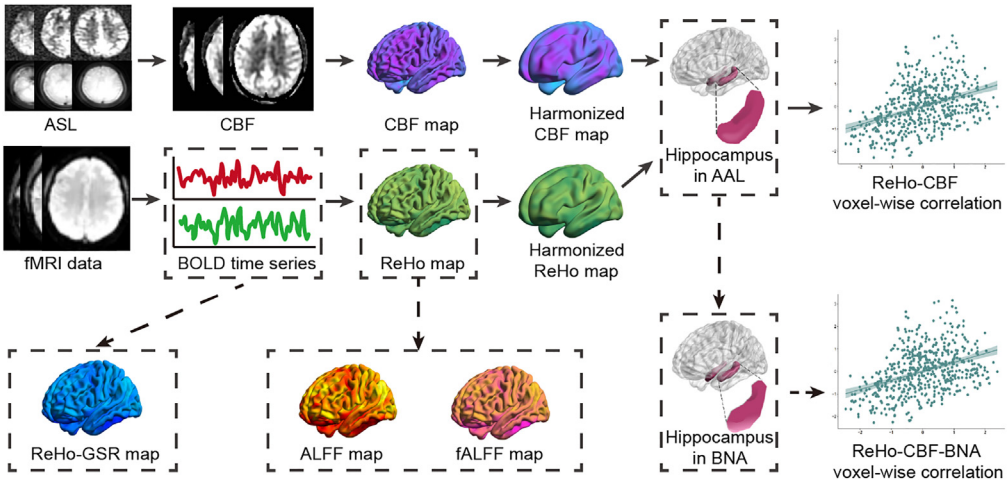

Figure 1. Calculation of the hippocampal BOLD-CBF correlation representing neurovascular coupling

(A–D) For each subject, the voxel-wise CBF map is calculated from ASL data and the voxel-wise ReHo map is computed from resting-state fMRI data without GSR. After ComBat harmonization, the harmonized CBF and ReHo maps are used to calculate the hippocampal BOLD-CBF correlation. The hippocampal voxels are extracted from the AAL and the hippocampal NVC is measured by BOLD-CBF correlation defined as the across-voxel correlation coefficient between ReHo and CBF in all hippocampal voxels. The hippocampal NVC is also calculated by other four approaches: (A) using ALFF to measure spontaneous neuronal activity; (B) using fALFF to measure spontaneous neuronal activity; (C) conducting GSR during the fMRI data preprocessing; (D) using the BNA to extract the hippocampal voxels. Abbreviations: AAL, automated anatomical atlas; ALFF, amplitude of low-frequency fluctuation; ASL, arterial spin labeling; BOLD, blood-oxygen-level-dependent; BNA, Brainnetome atlas; CBF, cerebral blood flow; fALFF, fractional ALFF; fMRI, functional magnetic resonance imaging; GSR, global signal regression; NVC, neurovascular coupling; ReHo, regional homogeneity.

In 100 subjects randomly selected from the discovery sample, we also tested the associations of ReHo-CBF correlation with the previously proposed resting-state fMRI NVC markers,[27] three shape parameters of the hemodynamic response function (HRF) including the response height (RH), time to peak (TTP), and full width at half maximum (FWHM). Across AAL regions, the correlations of ReHo-CBF coupling with the three shape parameters showed broad distributions (Figure S5), ranged from −0.62 to 0.68 for RH, from −0.37 to 0.25 for TTP, and from −0.34 to 0.25 for FWHM, indicating that the relations between ReHo-CBF coupling and HRF shape parameters are different across brain regions. For the bilateral hippocampal region, we found correlations of the ReHo-CBF coupling with TTP ($r = -0.47$, $p = 6.07 \times 10^{-7}$) and FWHM ($r = -0.28$, $p = 4.4 \times 10^{-4}$), but not with RH ($r = -0.17$, $p = 0.097$), indicating that ReHo-CBF coupling is partially associated with the latency and duration of HRF. In the 4,832 subjects, we also tested the correlation of the ReHo-CBF coupling with the absolute and relative volumes for the bilateral hippocampi and found that the ReHo-CBF coupling was not correlated with the absolute hippocampal volume ($r = -0.0016$, $p > 0.05$) but showed a weak correlation with relative hippocampal volume ($r = 0.052$, $p = 3.22 \times 10^{-4}$).

Heritability of the hippocampal blood-oxygen-level-dependent-cerebral blood flow correlation

We used the GREML-LDMS method[28] to estimate the single-nucleotide polymorphism (SNP) heritability (h^2) for the hippocampal BOLD-CBF correlation in the 4,832 unrelated individuals. In these subjects, the imputed 6,830,145 autosomal variants explained 20.7% (standard error (s.e.) = 7.6%) of the variance for the hippocampal BOLD-CBF correlation and the SNP heritability was significantly different from zero at the nominal 5% significance level ($p = 6.66 \times 10^{-3}$). When we used other four approaches to calculate the hippocampal BOLD-CBF correlation, the estimated h^2 values (16.2–23.9%, p = 0.001–0.024) for the hippocampal BOLD-CBF correlation were still significant (Table S3).

Genome-wide association studies of the hippocampal reginal homogeneity-cerebral blood flow correlation

A two-stage GWAS was conducted to find genetic associations with the hippocampal ReHo-CBF correlation, while controlling for age, age,[2] sex, age × sex, age[2] × sex, fMRI frame-wise displacement (FD), and the first ten genetic principal components. We used genome-wide significance ($p < 5 \times 10^{-8}$) as the discovery criterion and nominal significance ($p < 0.05$) as the replication criterion due to the small sample size. In the discovery stage (n = 4,406), we found two genome-wide significant loci associated with the hippocampal ReHo-CBF correlation with an inflation factor (λ_{GC}) of 1.005 indicating the well control of population substructure. One locus was at 3q28 with a lead SNP of rs13323015 ($p = 4.82 \times 10^{-8}$) and the other locus was at 12p11.22 with a lead SNP of rs10843101 ($p = 5.25 \times 10^{-9}$). In the replication stage (n = 426), the association of rs13323015 with the hippocampal ReHo-CBF correlation was replicated (consistent direction, $p = 5.79 \times 10^{-3}$), but we failed to replicate the association of rs10843101 with the hippocampal ReHo-CBF correlation (beta values in the same direction, p = 0.396). It was likely because limited sample size in the replication stage was difficult to have enough power to replicate the result, but it was found that association with lead SNP rs10843101 had the same direction of beta value, which was suggestive. We also conducted a GWAS meta-analysis to make full use of the available data to generate GWAS results for the gene-based association and enrichment analyses. We found that the

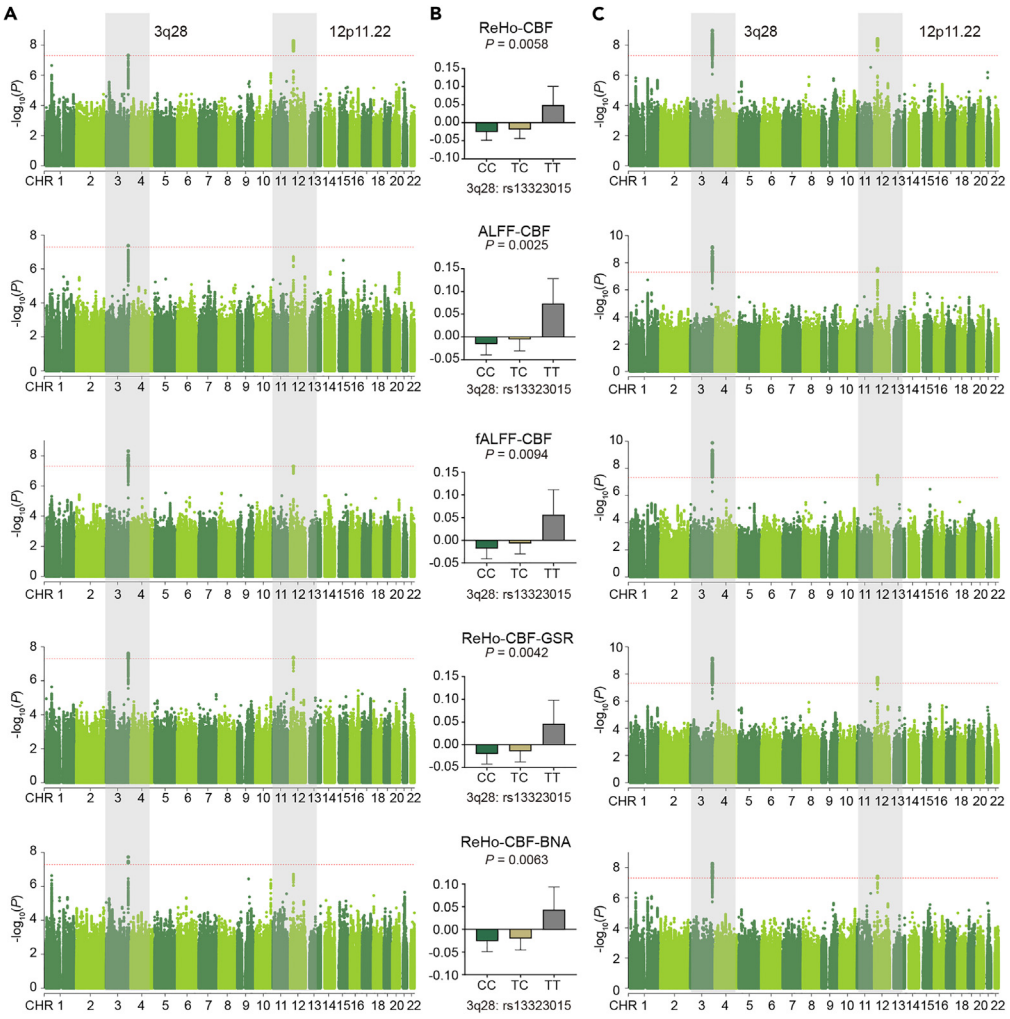

Figure 2. Genome-wide significant associations for the hippocampal BOLD-CBF correlation

(A) Manhattan plots show genome-wide significant associations (red line: $p = 5 \times 10^{-8}$) in the discovery stage for the hippocampal BOLD-CBF correlation measured by five methods. Each point represents a single genetic variant plotted according to its genomic position (x axis) and its -log10(*P*) value for the association (y axis).

(B) The comparisons of the hippocampal BOLD-CBF correlation among the genotypic groups of the lead variant (rs13323015 at 3q28) in replication stage and the y axis means the residuals of normalized hippocampal BOLD-CBF correlation while controlling for covariates used in genome-wide associations.

(C) Manhattan plots show genome-wide significant associations (red line: $p = 5 \times 10^{-8}$) in the meta-analysis for the hippocampal BOLD-CBF correlation measured by the five methods. Abbreviations: ALFF, amplitude of low-frequency fluctuation; BOLD, blood-oxygen-level-dependent; BNA, Brainnetome atlas; CBF, cerebral blood flow; CHR, chromosome; fALFF, fractional ALFF; GSR, global signal regression; NVC, neurovascular coupling; ReHo, regional homogeneity.

two loci identified in the discovery stage also showed genome-wide significant associations ($p = 1.79 \times 10^{-9}$ for the lead SNP rs13323015 at 3q28 and $p = 5.65 \times 10^{-9}$ for the lead SNP rs10843101 at 12p11.22) (Table S4) with the hippocampal ReHo-CBF correlation and quantile–quantile plots did not indicate genomic inflation ($\lambda_{GC} = 1.003$) (Figure 2).

Robustness of genome-wide association studies results

We also used other four approaches to calculate hippocampal BOLD-CBF correlation of these subjects and re-performed two-stage GWASs with the same covariates as the main analysis to confirm GWAS findings of the hippocampal ReHo-CBF correlation. In all the four analyses, the genome-wide significant association between rs13323015 at 3q28 and hippocampal BOLD-CBF correlation was confirmed in the discovery stage (n = 4,406; $p = 1.40–4.25 \times 10^{-8}$), replication stage (n = 426; consistent direction of effects, p = 0.0025–0.0094), and meta-analysis of the two stages (n = 4,832; $p = 5.34–8.04 \times 10^{-10}$) (Table S4). However, the association between rs10843101 at 12p11.22 and hippocampal BOLD-CBF correlation was not confirmed in the analyses (discovery stage: $p = 0.50–1.87 \times 10^{-7}$,

replication stage: p = 0.28–0.75, meta-analysis: p = 0.41–3.30 × 10^{-7}, Table S4). Although a few lead SNPs at 12p11.22 showed genome-wide significant association ($p < 5 \times 10^{-8}$) with hippocampal BOLD-CBF correlation in the discovery stage and/or meta-analysis, none of the tested associations was confirmed in the replication stage (all $p > 0.05$) (Table S5). Moreover, none of other SNPs outside the two loci reached genome-wide significant ($p < 5 \times 10^{-8}$) in any of these four GWASs (Figure 2). QQ-plots of the four GWASs showed good control of population substructure in both discovery and meta-analysis (λ_{GC} = 0.997–1.016, Figure S6). These results indicate that the association of 3q28 with hippocampal BOLD-CBF correlation is reproducible and the association of 12p11.22 with hippocampal BOLD-CBF correlation needs to be further confirmed in larger samples. We also used the CompCor approach[29] to remove white matter (WM) and cerebrospinal fluid (CSF) signals and then recalculated the ReHo maps, based on which we recalculated hippocampal ReHo-CBF correlation. We found significant correlation ($r = 0.95$, $p < 0.001$) between ReHo-CBF correlations in the hippocampal voxels derived from the two fMRI preprocessing approaches. We also re-performed GWAS in the 4,832 participants and found the same two loci with same lead SNPs of rs13081641 ($\beta = 0.139$, $p = 1.16 \times 10^{-9}$) and rs11049363 ($\beta = 0.1952$, $p = 9.06 \times 10^{-9}$, Figure S7). In addition, we used the same steps to conduct GWAS for the ReHo-CBF correlation of the bilateral precentral gyri defined by the AAL atlas in the 4,832 participants, however, we did not find any significant association at $p < 5 \times 10^{-8}$ (Figure S8). Compared with previous GWASs of the bilateral hippocampal volume,[30,31] there was not overlapping SNP between hippocampal ReHo-CBF correlation and hippocampal volume in mono-ancestry, but we found an overlapping SNP rs14474594 (3:190642839:A:G) in 3q28 near to *GMNC* (hippocampal ReHo-CBF correlation: $\beta = 0.13$, $p = 2.34 \times 10^{-8}$; right hippocampal volume: $\beta = 0.038$, $p = 2.18 \times 10^{-8}$; left hippocampal volume: $\beta = 0.042$, $p = 5.04 \times 10^{-10}$) between hippocampal ReHo-CBF correlation and bilateral hippocampal volume in cross-ancestry.[30]

Single- and multi-trait genome-wide association studies

In the 4,832 subjects, we also conducted GWAS for the hippocampal CBF and ReHo, respectively. Although we failed to identify genome-wide significant association for hippocampal ReHo (Figure S9A), we found a significant locus at 3q28 (rs78054167: $\beta = -0.14$, $p = 1.38 \times 10^{-9}$) for hippocampal CBF (Figure S9B). However, the effect was in the opposite direction compared to that for the ReHo-CBF correlation. We used three multivariate methods to conduct genetic association analyses by integrating the three neuroimaging phenotypes. Although the multi-trait analysis of GWAS (MTAG)[32] failed to find any significant genome-wide associations at $p < 5 \times 10^{-8}$ (Figure S9C), both CGWAS and MinGWAS[33] replicated our results (rs74712405 at 3q28: $p = 2.26 \times 10^{-10}$ in CGWAS, $p = 3.20 \times 10^{-9}$ in MinGWAS and rs11049363 at 12p11.22: $p = 2.81 \times 10^{-8}$ in CGWAS, $p = 1.16 \times 10^{-8}$ in MinGWAS, Figure S9D) but failed to find any new genetic associations.

Functional annotation for genome-wide association studies significant loci

In the main GWAS meta-analysis (ReHo-CBF), we found 183 genome-wide significant SNPs ($p < 5.0 \times 10^{-8}$) at 3q28 (lead SNP: rs74712405) and 12p11.22 (lead SNP: rs11049363) (Table S6; Figure S10). Most of the 152 genome-wide significant SNPs at 3q28 were mapped to an intergenic region between *GMNC* (Geminin Coiled-Coil Domain Containing) and *OSTN* (Osteocrin), of which 21 significant SNPs at 3q28 were associated with the expression of *GMNC* in the hippocampus from the Braineac dataset ($p = 0.03$–0.045, Table S7) and *GMNC* is an essential gene for neurogenesis after birth.[34] A portion of significant SNPs at 3q28 have been associated with neuroimaging markers (e.g., hippocampal CA1-body volume, fornix microstructure, and ventricle volume) and biomarkers (e.g., cerebrospinal P-tau level) of AD. The 31 significant SNPs of the suggestive locus (12p11.22) were mostly in the intergenic region between *PTHLH* (Parathyroid Hormone Like Hormone) and *CCDC91* (Coiled-Coil Domain Containing 91) and partly in the intronic region of *CCDC91*. Several SNPs have been associated with cortical surface area and thickness (Table S6). The HaploReg database showed that rs28380759 in strong linkage disequilibrium (LD) ($r^2 = 0.81$) with significant SNP rs10843111 was overlapped with the H3K4me3 promoter peaks in the hippocampus, indicative of transcriptionally active. Furthermore, rs10843111 was associated with the expression of *CCDC91* in the hippocampus ($p = 9.23 \times 10^{-16}$). Therefore, our results indicate a potential role of *GMNC* and *CCDC91* in regulating hippocampal ReHo-CBF correlation, however, further confirmation is needed.

Gene-based association analysis of the hippocampal blood-oxygen-level-dependent-cerebral blood flow correlation

We performed gene-based association analysis to identify genes associated with the hippocampal ReHo-CBF correlation in the 4,832 subjects and a Bonferroni method was used to adjust for the number of genes (n = 18,000) with a significant threshold of $p = 2.78 \times 10^{-6}$. We found that *GMNC* was the most significant gene associated with the hippocampal ReHo-CBF correlation ($p = 4.65 \times 10^{-11}$). Moreover, six additional genes including *CRTC2* (CREB Regulated Transcription Coactivator 2), *DENND4B* (DENN Domain Containing 4B), *CREB3L4* (CAMP Responsive Element Binding Protein 3 Like 4), *GATAD2B* (GATA Zinc Finger Domain Containing 2B), *SLC39A1* (Solute Carrier Family 39 Member 1) on chromosome 1, and *IL43* (Interleukin 34) on chromosome 16, were also significantly associated with the hippocampal ReHo-CBF correlation ($p < 2.78 \times 10^{-6}$). Based on the hippocampal BOLD-CBF correlation obtained from four additional methods, we re-performed gene-based association analyses with the same covariates and confirmed four genes that were consistently significant ($p < 2.78 \times 10^{-6}$) in these robustness analyses, including *GMNC*, *CRTC2*, *DENND4B*, and *GATAD2B* (Figure 3; Table S8).

Enrichment analyses

To gain more biological insight of the hippocampal BOLD-CBF correlation, we performed a series of enrichment analyses based on the main (ReHo-CBF) gene-based association results (18, 000 background genes). The tibial artery ($p = 0.0029$), coronary artery ($p = 0.0031$), and aorta

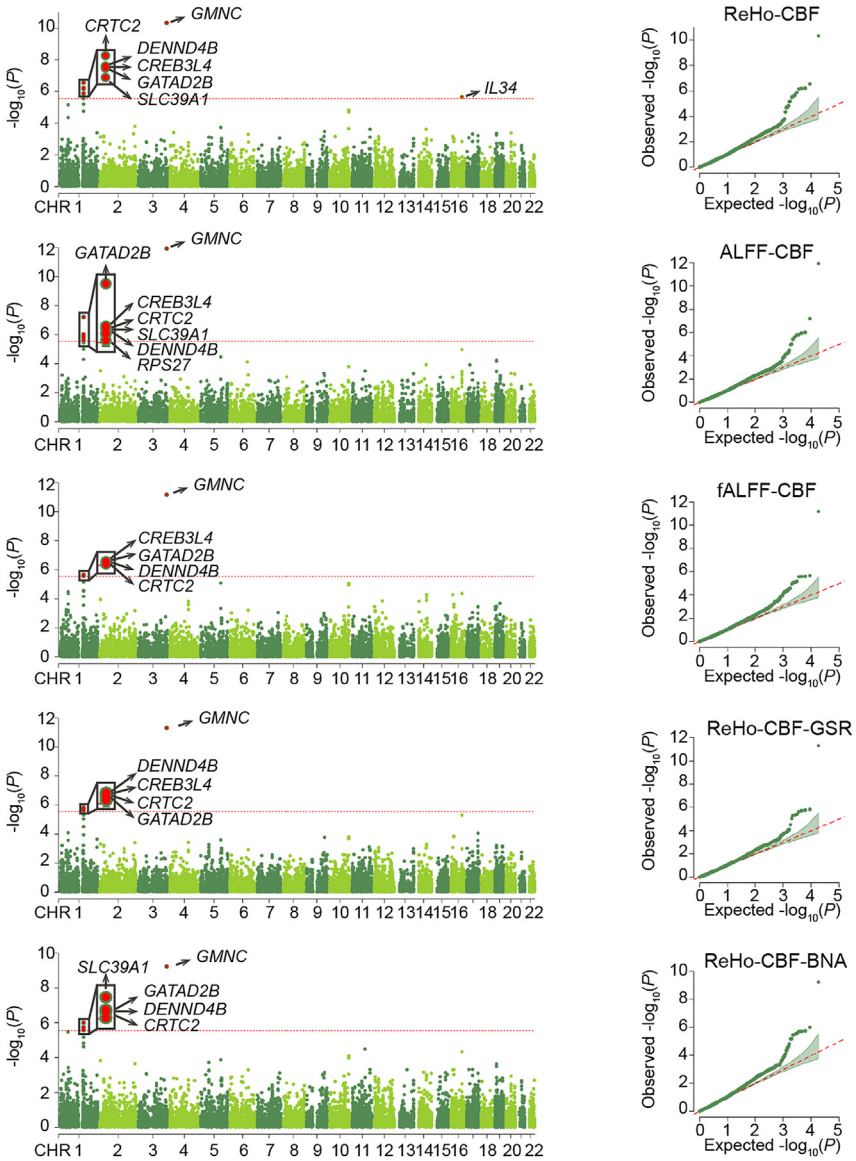

Figure 3. Genes associated with the hippocampal BOLD-CBF correlation in gene-based association analyses

Manhattan (left) and quantile-quantile (QQ) (right) plots show genes with significant associations with the hippocampal BOLD-CBF correlation in the gene-based association analyses. The red line indicates a Bonferroni-corrected threshold ($p = 2.78 \times 10^{-6}$) for gene-based analysis. Abbreviations: ALFF, amplitude of low-frequency fluctuation; BOLD, blood-oxygen-level-dependent; BNA, Brainnetome atlas; CBF, cerebral blood flow; CHR, chromosome; fALFF, fractional ALFF; GSR, global signal regression; NVC, neurovascular coupling; ReHo, regional homogeneity.

artery ($p = 0.0096$) were the top-ranked three items in the tissue-specific enrichment analysis (Figure 4A), of which only tibial artery was confirmed in all the four robustness analyses ($p < 0.05$, Table S9). The radial glia-like cells (RGCs) in the subventricular zone (SVZ-RGCs, $p = 0.0035$), RGCs in the dentate gyrus (DG-RGCs, $p = 0.0261$), and oligodendrocytes ($p = 0.0306$) showed nominally significant enrichment in the cell-specific enrichment analysis (Figure 4B), of which DG-RGCs were also nominally significant ($p = 0.0066$–0.0484) in three robustness analyses (Table S10). In the pathway enrichment analysis, we found five pathways with significant enrichment ($p < 4.88 \times 10^{-6}$, Bonferroni correction for the 10,226 pathways), including the pathways of the role of LAT2/NTAL/LAB on calcium mobilization, the negative regulation of activity of TFAP2 (AP-2) family of transcription factors, the microglial cell proliferation, the endosomal sorting complex required for transport (ESCRT) system, and the ubiquitin dependent protein catabolic process via the multivesicular body sorting pathway (Figure 4C; Table S11). Of these pathways, the LAT2/NTAL/LAB on calcium mobilization, microglial cell proliferation, and ESCRT system were confirmed in all robustness analyses ($p < 0.05$). In addition, we found 38 pathways with nominal significance ($p < 0.05$) in all the five pathway enrichment analyses (Table S12).

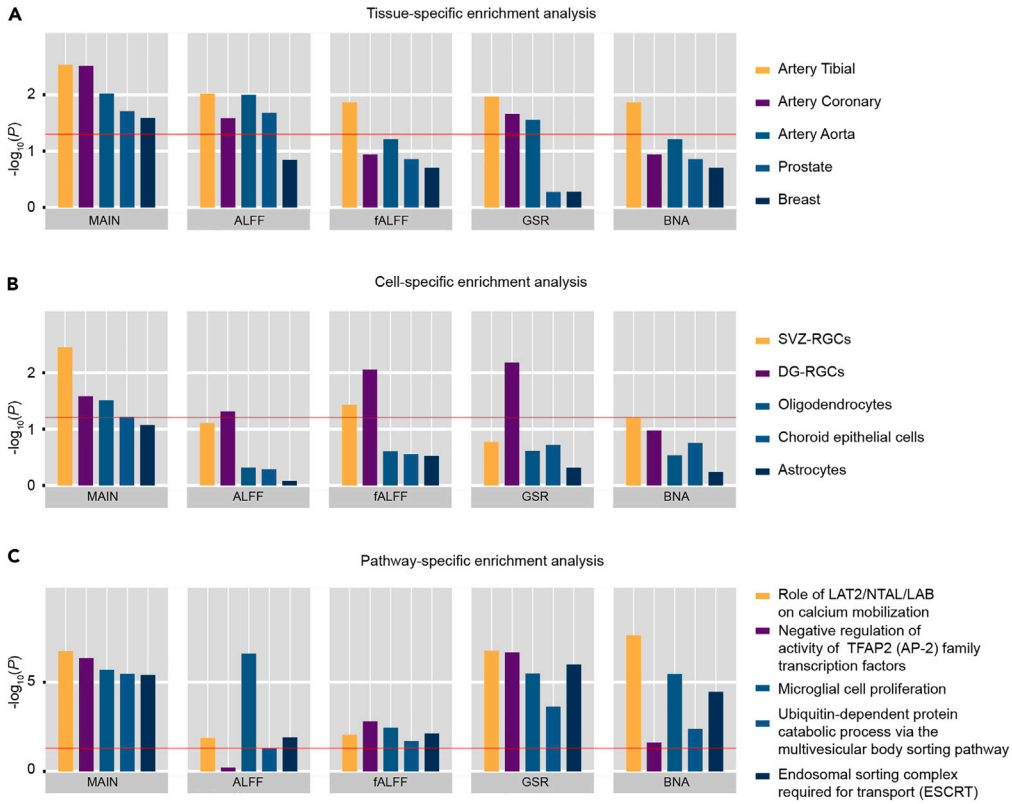

Figure 4. Enrichment analyses for genes associated with hippocampal BOLD-CBF correlation

(A) The top five tissue types enriched by genes associated with hippocampal BOLD-CBF correlation assessed by ReHo-CBF correlation (main analysis) and their significance in the robustness analyses. The y axis shows -log10(*P*) values, the x axis shows tissue types, the bar colors represent tissue types, and the red line means nominally significant threshold ($p < 0.05$).

(B) The top five cell types enriched by genes associated with hippocampal BOLD-CBF correlation (ReHo-CBF correlation) and their significance in the robustness analyses. The y axis shows -log10(*P*) values, the x axis shows cell types, and the same color represents same cell type. The red line means nominally significant threshold ($p < 0.05$).

(C) The top five pathways enriched by genes associated with hippocampal BOLD-CBF correlation (ReHo-CBF correlation) and their significance in the robustness analyses. The y axis represents -log10(*P*) values in pathway-specific enrichment analyses, and the x axis shows different pathways with different color bar. The red line means nominally significant threshold ($p < 0.05$). Abbreviations: ALFF, amplitude of low-frequency fluctuation; BOLD, blood-oxygen-level-dependent; BNA, Brainnetome atlas; CBF, cerebral blood flow; DG, dentate gyrus; fALFF, fractional ALFF; GSR, global signal regression; NVC, neurovascular coupling; ReHo, regional homogeneity; RGCs, radial glia-like cells; SVZ, subventricular zone.

DISCUSSION

This is the first GWAS to explore the genetic architecture of hippocampal BOLD-CBF correlation with an estimated heritability of 16.2–23.9%. We identified two genome-wide significant loci (3q28 and 12p11.22) associated with hippocampal BOLD-CBF correlation in 4,406 Chinese Han healthy individuals, of which the 3q28 was replicated in an independent sample of 426 subjects and confirmed by all the four robustness analyses. In gene-based association analyses, we discovered and confirmed four genes (*GMNC*, *DENND4B*, *CRTC2*, and *GATAD2B*) showing consistent associations with hippocampal BOLD-CBF correlation. The related genes enriched for vasculature, DG-RGCs, and biological pathways associated with calcium mobilization, microglial cell proliferation, and ESCRT system. These findings provide novel biological insight into the individual differences in hippocampal BOLD-CBF correlation.

The most important finding of this study was the discovery of a reliable association between the locus at 3q28 with the lead SNP of rs74712405 and the hippocampal BOLD-CBF correlation. Several significant SNPs in the locus have been associated with the biomarkers (such as cerebrospinal fluid P-tau level) and neuroimaging markers (e.g., cortical thickness and surface area, hippocampal and ventricular volumes, and white matter integrity) of AD.[35–45] For example, rs150434736 has been associated with the hippocampal CA1 volume[38]; and rs150434736, rs141962260 and rs12727448 were associated with the white matter microstructure in the fornix[38] that is the major output fibers of the hippocampus and the fractional anisotropy reduction in the fornix is an important feature of AD, even at an early stage of the disorder.[46] In terms of genes, we provided converging evidence for the association of *GMNC* with the hippocampal NVC, including significant SNPs at 3q28 were around *GMNC*; significant SNPs at 3q28 were associated with *GMNC* expression in the hippocampal tissue; and *GMNC* showed the strongest correlation with the hippocampal BOLD-CBF correlation in gene-based association analysis. *GMNC* also called *GEMC1* encode

Geminin coiled-coil domain-containing protein 1, which is essential for DNA replication[47] and regulates the balance between neural stem cell generation and ependymal cell differentiation in the postnatal brain.[34] We also found a suggestive locus at 12p11.22, which was mapped to *CCDC91*. *CCDC91* encoding p56, an accessory protein of the Golgi associated, γ-adaptin ear containing, Arf binding proteins (GGAs), is involved in transportation from Golgi to lysosome[48] and regulates the delivery of lysosomal enzymes in large neurons such as the hippocampal pyramidal neurons.[49]

In gene-based association analysis, we additionally identified three genes (*CRTC2*, *DENND4B*, *GATAD2B*) consistently associated with hippocampal BOLD-CBF correlation in all the five analyses. *DENND4B* is a GDP-GTP exchange factor (GEF) targeting to a tubular membrane compartment adjacent to the Golgi and activating RAB10[50] and RAB GTPases control membrane transport in neurons and astrocytes and are associated with cognitive functions and brain disorders including AD.[51] *GATAD2B* encodes a protein involved in chromatin modification and transcription regulation, which is required in neurons for normal cognitive performance and synapse development.[52] *CRTC2* encodes a member of the family of the cAMP-response element binding (CREB)-regulated transcription coactivators (CRTC), and the cAMP pathway can stabilize endothelial barrier and maintain vascular physiology. *CRTC2* was highly expressed in endothelial cells and related to angiogenesis acting as a protective molecule for the integrity of endothelium under ischemic condition.[53]

The significant enrichment of genes associated with the hippocampal BOLD-CBF correlation for vascular tissue may reflect that NVC is regulated by vascular component of the NVU. The significant enrichment for RGCs in subventricular zone and dentate gyrus, the only two regions with neurogenesis in adult brain,[54] indicates that the adulthood neurogenesis may be regulated by hippocampal BOLD-CBF correlation. We also identified three biological pathways associated with the genetic regulation of the hippocampal BOLD-CBF correlation in both main and robustness analyses. For example, the association of the hippocampal BOLD-CBF correlation with the regulatory pathway of mast cell calcium mobilization is consistent with the blood flow regulation of mast cells by releasing vasoactive substance[55] and the preferential location of mast cells in mature vessels surrounding by astrocytes,[56] two core components of the NVU. Microglial and endothelial cells are bidirectionally and permanently communicated with each other and excessive microglia response impairs endothelial cells, neurons, and astrocytes in the pathogenesis of many neurological disorders including AD,[57] supporting the link of the hippocampal NVC to the microglial cell proliferation. The ubiquitin-proteasome system of intracellular proteolysis is central to the regulation of cellular homeostasis including neurons, astrocytes, endothelial cells, all of which are the main components of the NVU. These mechanisms may underlie the associations of this system with brain functions (such as memory) and disorders (such as AD).[58,59]

In conclusion, this study identified one reliable locus (3q28) and four reliable genes (*GMNC*, *CRTC2*, *DENND4B*, and *GATAD2B*) associated with hippocampal BOLD-CBF correlation. Enrichment analyses indicate that the hippocampal BOLD-CBF correlation is regulated by several biological processes such as calcium mobilization by mast cells, ubiquitin-related proteolysis, and microglial cell proliferation, which impact the NVU components of neurons, astrocytes, and endothelial cells separately or in combination. These findings may improve our understanding of the genetic architecture underlying the hippocampal BOLD-CBF correlation and provide potential therapeutic targets for brain disorders with severe neurovascular uncoupling.

Limitation of the study

There are several limitations that should be mentioned in this study. First, there are lacking putative neuroimaging markers for *in vivo* assessment of NVC, although several proxies of NVC have been used previously.[27] The large variation between BOLD-CBF correlation and HRF shape parameters across brain regions further indicate that these neuroimaging markers may reflect different aspects of NVC. Second, although we conducted internal validation and sensitivity analyses, we cannot conduct external validation due to the lack of qualified neuroimaging datasets. Third, the sample size used in this study was small and only has power to detect common variants with very strong associations.

STAR★METHODS

Detailed methods are provided in the online version of this paper and include the following:

- KEY RESOURCES TABLE
- RESOURCE AVAILABILITY
  - Lead contact
  - Materials availability
  - Data and code availability
- EXPERIMENTAL MODEL AND STUDY PARTICIPANT DETAILS
- METHOD DETAILS
  - Subjects
  - Genotyping and imputation
  - Imaging data acquisition
  - Estimating parameters for spatial normalization
  - CBF calculation
  - fMRI data preprocessing and metric calculation
  - Quality assessment for spatial normalization

SUPPLEMENTAL INFORMATION

Supplemental information can be found online at https://doi.org/10.1016/j.isci.2023.108005.

ACKNOWLEDGMENTS

We are grateful to all participants and researchers of CHIMGEN study. We are grateful to the ENIGMA consortia for providing GWAS summary statistics of hippocampal volumes. This work was supported by the National Key Research and Development Program of China (2018YFC1314300), and the National Natural Science Foundation of China (82030053, 81425013). The authors report no biomedical financial interests or potential conflicts of interest. The funders had no role in study design, data collection and analysis, decision to publish, or preparation of the article.

AUTHOR CONTRIBUTIONS

C.Y. and H.X. designed the study and wrote the article. H.X., X.X., and Z.Y. analyzed the data. C.Y., J.X., Y.Y. supervised this work. H.X., X.X., Z.Y., J.C., L.Z., W.Z., G.C., Q.Z., S.Q., Z.Y., W.Q., F.L., M.L., J.F., Q.X., J.X., Y.X., P.Z., W.L., C.W., W.S., X.Z., K.X., X.Z., Z.Y., Y.Y., J.X. and C.Y. acquired the data. All authors critically reviewed the final version of the article.

DECLARATION OF INTERESTS

The authors declare that the research was conducted in the absence of any commercial or financial relationships that could be construed as a potential conflict of interest.

Received: March 6, 2023
Revised: July 29, 2023
Accepted: September 18, 2023
Published: September 21, 2023

REFERENCES

1. Logothetis, N.K., and Wandell, B.A. (2004). Interpreting the BOLD Signal. Annu. Rev. Physiol. *66*, 735–769. https://doi.org/10.1146/annurev.physiol.66.082602.092845.
2. Attwell, D., Buchan, A.M., Charpak, S., Lauritzen, M., Macvicar, B.A., and Newman, E.A. (2010). Glial and neuronal control of brain blood flow. Nature *468*, 232–243. https://doi.org/10.1038/nature09613.
3. Iadecola, C. (2017). The Neurovascular Unit Coming of Age: A Journey through Neurovascular Coupling in Health and Disease. Neuron *96*, 17–42. https://doi.org/10.1016/j.neuron.2017.07.030.
4. Phillips, A.A., Chan, F.H., Zheng, M.M.Z., Krassioukov, A.V., and Ainslie, P.N. (2016). Neurovascular coupling in humans: Physiology, methodological advances and clinical implications. J. Cereb. Blood Flow Metab. *36*, 647–664. https://doi.org/10.1177/0271678x15617954.
5. Ouellette, J., Toussay, X., Comin, C.H., Costa, L.D.F., Ho, M., Lacalle-Aurioles, M., Freitas-Andrade, M., Liu, Q.Y., Leclerc, S., Pan, Y., et al. (2020). Vascular contributions to 16p11.2 deletion autism syndrome modeled in mice. Nat. Neurosci. *23*, 1090–1101. https://doi.org/10.1038/s41593-020-0663-1.
6. Baller, E.B., Valcarcel, A.M., Adebimpe, A., Alexander-Bloch, A., Cui, Z., Gur, R.C., Gur, R.E., Larsen, B.L., Linn, K.A., O'Donnell, C.M., et al. (2022). Developmental coupling of cerebral blood flow and fMRI fluctuations in youth. Cell Rep. *38*, 110576. ARTN 110576. https://doi.org/10.1016/j.celrep.2022.110576.
7. Li, H., Huang, Z., Gao, Z., Zhu, W., Li, Y., Zhou, S., Li, X., and Yu, Y. (2023). Sex Difference in General Cognition Associated with Coupling of Whole-brain Functional Connectivity Strength to Cerebral Blood Flow Changes During Alzheimer's Disease Progression. Neuroscience *509*, 187–200. https://doi.org/10.1016/j.neuroscience.2022.12.001.
8. Zhu, J., Zhuo, C., Xu, L., Liu, F., Qin, W., and Yu, C. (2017). Altered Coupling Between Resting-State Cerebral Blood Flow and Functional Connectivity in Schizophrenia. Schizophr. Bull. *43*, 1363–1374. https://doi.org/10.1093/schbul/sbx051.
9. Su, S., Zhao, J., Dai, Y., Lin, L., Zhou, Q., Yan, Z., Qian, L., Cui, W., Liu, M., Zhang, H., et al. (2023). Altered neurovascular coupling in the children with attention-deficit/hyperactivity disorder: a comprehensive fMRI analysis. Eur. Child Adolesc. Psychiatry, 1–11. https://doi.org/10.1007/s00787-023-02238-0.
10. Liu, X., Cheng, R., Chen, L., Gong, J., Luo, T., and Lv, F. (2021). Altered Neurovascular Coupling in Subcortical Ischemic Vascular Disease. Front. Aging Neurosci. *13*, 598365. https://doi.org/10.3389/fnagi.2021.598365.
11. Bird, C.M., and Burgess, N. (2008). The hippocampus and memory: insights from spatial processing. Nat. Rev. Neurosci. *9*, 182–194. https://doi.org/10.1038/nrn2335.
12. Rolls, E.T., and Wirth, S. (2018). Spatial representations in the primate hippocampus, and their functions in memory and navigation. Prog. Neurobiol. *171*, 90–113. https://doi.org/10.1016/j.pneurobio.2018.09.004.
13. Mu, Y., and Gage, F.H. (2011). Adult hippocampal neurogenesis and its role in Alzheimer's disease. Mol. Neurodegener. *6*, 85. https://doi.org/10.1186/1750-1326-6-85.
14. Heckers, S., and Konradi, C. (2010). Hippocampal pathology in schizophrenia. Curr. Top. Behav. Neurosci. *4*, 529–553. https://doi.org/10.1007/7854_2010_43.

15. Shen, J., Wang, D., Wang, X., Gupta, S., Ayloo, B., Wu, S., Prasad, P., Xiong, Q., Xia, J., and Ge, S. (2019). Neurovascular Coupling in the Dentate Gyrus Regulates Adult Hippocampal Neurogenesis. Neuron *103*, 878–890.e3. https://doi.org/10.1016/j.neuron.2019.05.045.
16. Lazarov, O., and Hollands, C. (2016). Hippocampal neurogenesis: Learning to remember. Prog. Neurobiol. *138–140*, 1–18. https://doi.org/10.1016/j.pneurobio.2015.12.006.
17. Shaw, K., Bell, L., Boyd, K., Grijseels, D.M., Clarke, D., Bonnar, O., Crombag, H.S., and Hall, C.N. (2021). Neurovascular coupling and oxygenation are decreased in hippocampus compared to neocortex because of microvascular differences. Nat. Commun. *12*, 3190. https://doi.org/10.1038/s41467-021-23508-y.
18. Kisler, K., Nelson, A.R., Montagne, A., and Zlokovic, B.V. (2017). Cerebral blood flow regulation and neurovascular dysfunction in Alzheimer disease. Nat. Rev. Neurosci. *18*, 419–434. https://doi.org/10.1038/nrn.2017.48.
19. Li, L., Tong, X.K., Hosseini Kahnouei, M., Vallerand, D., Hamel, E., and Girouard, H. (2021). Impaired Hippocampal Neurovascular Coupling in a Mouse Model of Alzheimer's Disease. Front. Physiol. *12*, 715446. https://doi.org/10.3389/fphys.2021.715446.
20. Dunlop, K., and Liston, C. (2018). Stress response regulation and the hemodynamic response. Proc. Natl. Acad. Sci. USA *115*, 10827–10829. https://doi.org/10.1073/pnas.1814592115.
21. Hu, B., Yan, L.F., Sun, Q., Yu, Y., Zhang, J., Dai, Y.J., Yang, Y., Hu, Y.C., Nan, H.Y., Zhang, X., et al. (2019). Disturbed neurovascular coupling in type 2 diabetes mellitus patients: Evidence from a comprehensive fMRI analysis. Neuroimage. Clin. *22*, 101802. https://doi.org/10.1016/j.nicl.2019.101802.
22. Xu, Q., Guo, L., Cheng, J., Wang, M., Geng, Z., Zhu, W., Zhang, B., Liao, W., Qiu, S., Zhang, H., et al. (2020). CHIMGEN: a Chinese imaging genetics cohort to enhance cross-ethnic and cross-geographic brain research. Mol. Psychiatry *25*, 517–529. https://doi.org/10.1038/s41380-019-0627-6.
23. Reig, S., Sánchez-González, J., Arango, C., Castro, J., González-Pinto, A., Ortuño, F., Crespo-Facorro, B., Bargalló, N., and Desco, M. (2009). Assessment of the increase in variability when combining volumetric data from different scanners. Hum. Brain Mapp. *30*, 355–368. https://doi.org/10.1002/hbm.20511.
24. Rolls, E.T., Joliot, M., and Tzourio-Mazoyer, N. (2015). Implementation of a new parcellation of the orbitofrontal cortex in the automated anatomical labeling atlas. Neuroimage *122*, 1–5. https://doi.org/10.1016/j.neuroimage.2015.07.075.
25. Fortin, J.P., Cullen, N., Sheline, Y.I., Taylor, W.D., Aselcioglu, I., Cook, P.A., Adams, P., Cooper, C., Fava, M., McGrath, P.J., et al. (2018). Harmonization of cortical thickness measurements across scanners and sites. Neuroimage *167*, 104–120. https://doi.org/10.1016/j.neuroimage.2017.11.024.
26. Fan, L., Li, H., Zhuo, J., Zhang, Y., Wang, J., Chen, L., Yang, Z., Chu, C., Xie, S., Laird, A.R., et al. (2016). The Human Brainnetome Atlas: A New Brain Atlas Based on Connectional Architecture. Cereb. Cortex *26*, 3508–3526. https://doi.org/10.1093/cercor/bhw157.
27. Wu, G.R., Colenbier, N., Van Den Bossche, S., Clauw, K., Johri, A., Tandon, M., and Marinazzo, D. (2021). rsHRF: A toolbox for resting-state HRF estimation and deconvolution. Neuroimage *244*, 118591. https://doi.org/10.1016/j.neuroimage.2021.118591.
28. Yang, J., Bakshi, A., Zhu, Z., Hemani, G., Vinkhuyzen, A.A.E., Lee, S.H., Robinson, M.R., Perry, J.R.B., Nolte, I.M., van Vliet-Ostaptchouk, J.V., et al. (2015). Genetic variance estimation with imputed variants finds negligible missing heritability for human height and body mass index. Nat. Genet. *47*, 1114–1120. https://doi.org/10.1038/ng.3390.
29. Behzadi, Y., Restom, K., Liau, J., and Liu, T.T. (2007). A component based noise correction method (CompCor) for BOLD and perfusion based fMRI. Neuroimage *37*, 90–101. https://doi.org/10.1016/j.neuroimage.2007.04.042.
30. Liu, N., Zhang, L., Tian, T., Cheng, J., Zhang, B., Qiu, S., Geng, Z., Cui, G., Zhang, Q., Liao, W., et al. (2023). Cross-ancestry genome-wide association meta-analyses of hippocampal and subfield volumes. Nat. Genet. *55*, 1126–1137. https://doi.org/10.1038/s41588-023-01425-8.
31. Hibar, D.P., Adams, H.H.H., Jahanshad, N., Chauhan, G., Stein, J.L., Hofer, E., Renteria, M.E., Bis, J.C., Arias-Vasquez, A., Ikram, M.K., et al. (2017). Novel genetic loci associated with hippocampal volume. Nat. Commun. *8*, 13624. https://doi.org/10.1038/ncomms13624.
32. Turley, P., Walters, R.K., Maghzian, O., Okbay, A., Lee, J.J., Fontana, M.A., Nguyen-Viet, T.A., Wedow, R., Zacher, M., Furlotte, N.A., et al. (2018). Multi-trait analysis of genome-wide association summary statistics using MTAG. Nat. Genet. *50*, 229–237. https://doi.org/10.1038/s41588-017-0009-4.
33. Xiong, Z., Gao, X., Chen, Y., Feng, Z., Pan, S., Lu, H., Uitterlinden, A.G., Nijsten, T., Ikram, A., Rivadeneira, F., et al. (2022). Combining genome-wide association studies highlight novel loci involved in human facial variation. Nat. Commun. *13*, 7832. https://doi.org/10.1038/s41467-022-35328-9.
34. Lalioti, M.E., Kaplani, K., Lokka, G., Georgomanolis, T., Kyrousi, C., Dong, W., Dunbar, A., Parlapani, E., Damianidou, E., Spassky, N., et al. (2019). GemC1 is a critical switch for neural stem cell generation in the postnatal brain. Glia *67*, 2360–2373. https://doi.org/10.1002/glia.23690.
35. van der Meer, D., Frei, O., Kaufmann, T., Shadrin, A.A., Devor, A., Smeland, O.B., Thompson, W.K., Fan, C.C., Holland, D., Westlye, L.T., et al. (2020). Understanding the genetic determinants of the brain with MOSTest. Nat. Commun. *11*, 3512. https://doi.org/10.1038/s41467-020-17368-1.
36. Vojinovic, D., Adams, H.H., Jian, X., Yang, Q., Smith, A.V., Bis, J.C., Teumer, A., Scholz, M., Armstrong, N.J., Hofer, E., et al. (2018). Genome-wide association study of 23,500 individuals identifies 7 loci associated with brain ventricular volume. Nat. Commun. *9*, 3945. https://doi.org/10.1038/s41467-018-06234-w.
37. Zhao, B., Luo, T., Li, T., Li, Y., Zhang, J., Shan, Y., Wang, X., Yang, L., Zhou, F., Zhu, Z., et al. (2019). Genome-wide association analysis of 19,629 individuals identifies variants influencing regional brain volumes and refines their genetic co-architecture with cognitive and mental health traits. Nat. Genet. *51*, 1637–1644. https://doi.org/10.1038/s41588-019-0516-6.
38. Smith, S.M., Douaud, G., Chen, W., Hanayik, T., Alfaro-Almagro, F., Sharp, K., and Elliott, L.T. (2021). An expanded set of genome-wide association studies of brain imaging phenotypes in UK Biobank. Nat. Neurosci. *24*, 737–745. https://doi.org/10.1038/s41593-021-00826-4.
39. Zhao, B., Zhang, J., Ibrahim, J.G., Luo, T., Santelli, R.C., Li, Y., Li, T., Shan, Y., Zhu, Z., Zhou, F., et al. (2021). Large-scale GWAS reveals genetic architecture of brain white matter microstructure and genetic overlap with cognitive and mental health traits (n = 17,706). Mol. Psychiatry *26*, 3943–3955. https://doi.org/10.1038/s41380-019-0569-z.
40. Elvsåshagen, T., Shadrin, A., Frei, O., van der Meer, D., Bahrami, S., Kumar, V.J., Smeland, O., Westlye, L.T., Andreassen, O.A., and Kaufmann, T. (2021). The genetic architecture of the human thalamus and its overlap with ten common brain disorders. Nat. Commun. *12*, 2909. https://doi.org/10.1038/s41467-021-23175-z.
41. Shadrin, A.A., Kaufmann, T., van der Meer, D., Palmer, C.E., Makowski, C., Loughnan, R., Jernigan, T.L., Seibert, T.M., Hagler, D.J., Smeland, O.B., et al. (2021). Vertex-wise multivariate genome-wide association study identifies 780 unique genetic loci associated with cortical morphology. Neuroimage *244*, 118603. https://doi.org/10.1016/j.neuroimage.2021.118603.
42. van der Meer, D., Kaufmann, T., Shadrin, A.A., Makowski, C., Frei, O., Roelfs, D., Monereo-Sánchez, J., Linden, D.E.J., Rokicki, J., Alnæs, D., et al. (2021). The genetic architecture of human cortical folding. Sci. Adv. *7*, eabj9446. https://doi.org/10.1126/sciadv.abj9446.
43. Naqvi, S., Sleyp, Y., Hoskens, H., Indencleef, K., Spence, J.P., Bruffaerts, R., Radwan, A., Eller, R.J., Richmond, S., Shriver, M.D., et al. (2021). Shared heritability of human face and brain shape. Nat. Genet. *53*, 830–839. https://doi.org/10.1038/s41588-021-00827-w.
44. Deming, Y., Li, Z., Kapoor, M., Harari, O., Del-Aguila, J.L., Black, K., Carrell, D., Cai, Y., Fernandez, M.V., Budde, J., et al. (2017). Genome-wide association study identifies four novel loci associated with Alzheimer's endophenotypes and disease modifiers. Acta Neuropathol. *133*, 839–856. https://doi.org/10.1007/s00401-017-1685-y.
45. Hofer, E., Roshchupkin, G.V., Adams, H.H.H., Knol, M.J., Lin, H., Li, S., Zare, H., Ahmad, S., Armstrong, N.J., Satizabal, C.L., et al. (2020). Genetic correlations and genome-wide associations of cortical structure in general population samples of 22,824 adults. Nat. Commun. *11*, 4796. https://doi.org/10.1038/s41467-020-18367-y.
46. Kantarci, K. (2014). Fractional anisotropy of the fornix and hippocampal atrophy in Alzheimer's disease. Front. Aging Neurosci. *6*, 316. https://doi.org/10.3389/fnagi.2014.00316.
47. Balestrini, A., Cosentino, C., Errico, A., Garner, E., and Costanzo, V. (2010). GEMC1 is a TopBP1-interacting protein required for chromosomal DNA replication. Nat. Cell Biol. *12*, 484–491. https://doi.org/10.1038/ncb2050.
48. Mardones, G.A., Burgos, P.V., Brooks, D.A., Parkinson-Lawrence, E., Mattera, R., and Bonifacino, J.S. (2007). The trans-Golgi network accessory protein p56 promotes long-range movement of GGA/clathrin-containing transport carriers and lysosomal enzyme sorting. Mol. Biol. Cell *18*, 3486–3501. https://doi.org/10.1091/mbc.e07-02-0190.

49. Uemura, T., Sawada, N., Sakaba, T., Kametaka, S., Yamamoto, M., and Waguri, S. (2018). Intracellular localization of GGA accessory protein p56 in cell lines and central nervous system neurons. Biomed. Res. *39*, 179–187. https://doi.org/10.2220/biomedres.39.179.
50. Yoshimura, S.i., Gerondopoulos, A., Linford, A., Rigden, D.J., and Barr, F.A. (2010). Family-wide characterization of the DENN domain Rab GDP-GTP exchange factors. J. Cell Biol. *191*, 367–381. https://doi.org/10.1083/jcb.201008051.
51. D'Adamo, P., Masetti, M., Bianchi, V., Morè, L., Mignogna, M.L., Giannandrea, M., and Gatti, S. (2014). RAB GTPases and RAB-interacting proteins and their role in the control of cognitive functions. Neurosci. Biobehav. Rev. *46 Pt 2*, 302–314. https://doi.org/10.1016/j.neubiorev.2013.12.009.
52. Willemsen, M.H., Nijhof, B., Fenckova, M., Nillesen, W.M., Bongers, E.M.H.F., Castells-Nobau, A., Asztalos, L., Viragh, E., van Bon, B.W.M., Tezel, E., et al. (2013). GATAD2B loss-of-function mutations cause a recognisable syndrome with intellectual disability and are associated with learning deficits and synaptic undergrowth in Drosophila. J. Med. Genet. *50*, 507–514. https://doi.org/10.1136/jmedgenet-2012-101490.
53. Kanki, H., Sasaki, T., Matsumura, S., Kawano, T., Todo, K., Okazaki, S., Nishiyama, K., Takemori, H., and Mochizuki, H. (2020). CREB Coactivator CRTC2 Plays a Crucial Role in Endothelial Function. J. Neurosci. *40*, 9533–9546. https://doi.org/10.1523/jneurosci.0407-20.2020.
54. Niklison-Chirou, M.V., Agostini, M., Amelio, I., and Melino, G. (2020). Regulation of Adult Neurogenesis in Mammalian Brain. Int. J. Mol. Sci. *21*, 4869. https://doi.org/10.3390/ijms21144869.
55. Khalil, M., Ronda, J., Weintraub, M., Jain, K., Silver, R., and Silverman, A.J. (2007). Brain mast cell relationship to neurovasculature during development. Brain Res. *1171*, 18–29. https://doi.org/10.1016/j.brainres.2007.07.034.
56. Kunder, C.A., St John, A.L., and Abraham, S.N. (2011). Mast cell modulation of the vascular and lymphatic endothelium. Blood *118*, 5383–5393. https://doi.org/10.1182/blood-2011-07-358432.
57. Dudvarski Stankovic, N., Teodorczyk, M., Ploen, R., Zipp, F., and Schmidt, M.H.H. (2016). Microglia-blood vessel interactions: a double-edged sword in brain pathologies. Acta Neuropathol. *131*, 347–363. https://doi.org/10.1007/s00401-015-1524-y.
58. Lip, P.Z.Y., Demasi, M., and Bonatto, D. (2017). The role of the ubiquitin proteasome system in the memory process. Neurochem. Int. *102*, 57–65. https://doi.org/10.1016/j.neuint.2016.11.013.
59. Harris, L.D., Jasem, S., and Licchesi, J.D.F. (2020). The Ubiquitin System in Alzheimer's Disease. Adv. Exp. Med. Biol. *1233*, 195–221. https://doi.org/10.1007/978-3-030-38266-7_8.
60. Chang, C.C., Chow, C.C., Tellier, L.C., Vattikuti, S., Purcell, S.M., and Lee, J.J. (2015). Second-generation PLINK: rising to the challenge of larger and richer datasets. GigaScience *4*, 7. https://doi.org/10.1186/s13742-015-0047-8.
61. Willer, C.J., Li, Y., and Abecasis, G.R. (2010). METAL: fast and efficient meta-analysis of genomewide association scans. Bioinformatics *26*, 2190–2191. https://doi.org/10.1093/bioinformatics/btq340.
62. Pruim, R.J., Welch, R.P., Sanna, S., Teslovich, T.M., Chines, P.S., Gliedt, T.P., Boehnke, M., Abecasis, G.R., and Willer, C.J. (2010). LocusZoom: regional visualization of genome-wide association scan results. Bioinformatics *26*, 2336–2337. https://doi.org/10.1093/bioinformatics/btq419.
63. Wang, K., Li, M., and Hakonarson, H. (2010). ANNOVAR: functional annotation of genetic variants from high-throughput sequencing data. Nucleic Acids Res. *38*, e164. https://doi.org/10.1093/nar/gkq603.
64. de Leeuw, C.A., Mooij, J.M., Heskes, T., and Posthuma, D. (2015). MAGMA: generalized gene-set analysis of GWAS data. PLoS Comput. Biol. *11*, e1004219. https://doi.org/10.1371/journal.pcbi.1004219.
65. Delaneau, O., Zagury, J.F., and Marchini, J. (2013). Improved whole-chromosome phasing for disease and population genetic studies. Nat. Methods *10*, 5–6. https://doi.org/10.1038/nmeth.2307.
66. Howie, B.N., Donnelly, P., and Marchini, J. (2009). A flexible and accurate genotype imputation method for the next generation of genome-wide association studies. PLoS Genet. *5*, e1000529. https://doi.org/10.1371/journal.pgen.1000529.
67. 1000 Genomes Project Consortium, Auton, A., Brooks, L.D., Durbin, R.M., Garrison, E.P., Kang, H.M., Korbel, J.O., Marchini, J.L., McCarthy, S., McVean, G.A., and Abecasis, G.R. (2015). A global reference for human genetic variation. Nature *526*, 68–74. https://doi.org/10.1038/nature15393.
68. Wu, D., Dou, J., Chai, X., Bellis, C., Wilm, A., Shih, C.C., Soon, W.W.J., Bertin, N., Lin, C.B., Khor, C.C., et al. (2019). Large-Scale Whole-Genome Sequencing of Three Diverse Asian Populations in Singapore. Cell *179*, 736–749.e15. https://doi.org/10.1016/j.cell.2019.09.019.
69. Wells, W.M., Grimson, W.L., Kikinis, R., and Jolesz, F.A. (1996). Adaptive segmentation of MRI data. IEEE Trans. Med. Imaging *15*, 429–442. https://doi.org/10.1109/42.511747.
70. Ashburner, J. (2007). A fast diffeomorphic image registration algorithm. Neuroimage *38*, 95–113. https://doi.org/10.1016/j.neuroimage.2007.07.007.
71. Greve, D.N., and Fischl, B. (2009). Accurate and robust brain image alignment using boundary-based registration. Neuroimage *48*, 63–72. https://doi.org/10.1016/j.neuroimage.2009.06.060.
72. Zang, Y., Jiang, T., Lu, Y., He, Y., and Tian, L. (2004). Regional homogeneity approach to fMRI data analysis. Neuroimage *22*, 394–400. https://doi.org/10.1016/j.neuroimage.2003.12.030.
73. Zang, Y.F., He, Y., Zhu, C.Z., Cao, Q.J., Sui, M.Q., Liang, M., Tian, L.X., Jiang, T.Z., and Wang, Y.F. (2007). Altered baseline brain activity in children with ADHD revealed by resting-state functional MRI. Brain Dev. *29*, 83–91. https://doi.org/10.1016/j.braindev.2006.07.002.
74. Zou, Q.H., Zhu, C.Z., Yang, Y., Zuo, X.N., Long, X.Y., Cao, Q.J., Wang, Y.F., and Zang, Y.F. (2008). An improved approach to detection of amplitude of low-frequency fluctuation (ALFF) for resting-state fMRI: fractional ALFF. J. Neurosci. Methods *172*, 137–141. https://doi.org/10.1016/j.jneumeth.2008.04.012.
75. Liu, T.T., Nalci, A., and Falahpour, M. (2017). The global signal in fMRI: Nuisance or Information? Neuroimage *150*, 213–229.
76. Ward, L.D., and Kellis, M. (2016). HaploReg v4: systematic mining of putative causal variants, cell types, regulators and target genes for human complex traits and disease. Nucleic Acids Res. *44*, D877–D881. https://doi.org/10.1093/nar/gkv1340.
77. Boyle, A.P., Hong, E.L., Hariharan, M., Cheng, Y., Schaub, M.A., Kasowski, M., Karczewski, K.J., Park, J., Hitz, B.C., Weng, S., et al. (2012). Annotation of functional variation in personal genomes using RegulomeDB. Genome Res. *22*, 1790–1797. https://doi.org/10.1101/gr.137323.112.
78. Zheng, Z., Huang, D., Wang, J., Zhao, K., Zhou, Y., Guo, Z., Zhai, S., Xu, H., Cui, H., Yao, H., et al. (2020). QTLbase: an integrative resource for quantitative trait loci across multiple human molecular phenotypes. Nucleic Acids Res. *48*, D983–D991. https://doi.org/10.1093/nar/gkz888.
79. GTEx Consortium (2020). The GTEx Consortium atlas of genetic regulatory effects across human tissues. Science *369*, 1318–1330. https://doi.org/10.1126/science.aaz1776.
80. Zeisel, A., Hochgerner, H., Lönnerberg, P., Johnsson, A., Memic, F., van der Zwan, J., Häring, M., Braun, E., Borm, L.E., La Manno, G., et al. (2018). Molecular Architecture of the Mouse Nervous System. Cell *174*, 999–1014.e22. https://doi.org/10.1016/j.cell.2018.06.021.
81. Bryois, J., Skene, N.G., Hansen, T.F., Kogelman, L.J.A., Watson, H.J., Liu, Z.; Eating Disorders Working Group of the Psychiatric Genomics Consortium; International Headache Genetics Consortium; 23andMe Research Team, and Brueggeman, L., et al. (2020). Genetic identification of cell types underlying brain complex traits yields insights into the etiology of Parkinson's disease. Nat. Genet. *52*, 482–493. https://doi.org/10.1038/s41588-020-0610-9.

STAR★METHODS

KEY RESOURCES TABLE

REAGENT or RESOURCE	SOURCE	IDENTIFIER
Deposited data		
GWAS Summary statistics	This study	https://doi.org/10.6084/m9.figshare.23551605.v1
Individual level genotype, imputed markers and MRI data	The CHIMGEN study	http://chimgen.tmu.edu.cn/
Software and algorithms		
Matlab 2017b	Mathworks	https://login.mathworks.com/embedded-login/landing.html?cid=getmatlab&s_tid=gn_getml
R 4.1.3	R Foundation	https://cran.r-project.org/bin/linux/
Python 3.11.0	Python Software Foundation	https://www.python.org/
rsHRF Matlab toolbox	Wu et al.[27]	https://github.com/compneuro-da/rsHRF
GCTA-LDMS	Yang et al.[28]	https://yanglab.westlake.edu.cn/software/gcta/#GREMLinWGSorimputeddata
PLINK v2.0	Chang et al.[60]	https://www.cog-genomics.org/plink/2.0/
METAL	Willer et al.[61]	http://csg.sph.umich.edu/abecasis/Metal/
LocusZoom	Pruim et al.[62]	http://locuszoom.org/
ANNOVAR	Wang et al.[63]	https://annovar.openbioinformatics.org/en/latest/
MTAG	Turley et al.[32]	https://github.com/JonJala/mtag
CGWAS	Xiong et al.[33]	https://github.com/TianTTL/CGWAS
MAGMA v1.09	de Leeuw et al.[64]	https://ctg.cncr.nl/software/magma

RESOURCE AVAILABILITY

Lead contact

Further information and requests for resources and reagents should be directed to and will be fulfilled by the lead contact, Chunshui Yu (chunshuiyu@tmu.edu.cn).

Materials availability

This study did not generate new unique reagents.

Data and code availability

- The raw brain imaging and genotype data are available from the authors upon reasonable request and with permissions of the CHIMGEN consortia. The raw brain imaging and genotype data reported in this study cannot be deposited in a public repository because the local raw. To request access, the raw data was available with the permission of the CHIMGEN consortia by contact with lead contact. In addition, the GWAS summary for hippocampal BOLD-CBF correlation have been deposited at https://doi.org/10.6084/m9.figshare.23551605.v1 and is publicly available as of the date of publication.
- This paper does not report original code. We made use of publicly available software and tools in this study. All relevant software and code are described in the text and can be found at the URLs or references cited.
- Any additional information required to reanalyze the data reported in this paper is available from the lead contact upon request

EXPERIMENTAL MODEL AND STUDY PARTICIPANT DETAILS

This study reports the results of a GWAS conducted on 48,32 Chinese Han subjects. The procedure including recruitment and quality control of data are described in the method details section. The demographic characteristics are reported in Table S1. The study was approved by the Ethics Committee of each site, and all participants signed the written informed consent.

METHOD DETAILS

Subjects

All subjects were recruited from the CHIMGEN study, which has collected genomic and neuroimaging data from 7,306 healthy Chinese Han individuals aged 18 to 30 from 32 centers in 21 cities.[22] The protocols of the CHIMGEN study were approved by the ethics committee of each site, and written informed consent was obtained from each subject. The inclusion and exclusion criteria of the CHIMGEN subjects are provided in Table S13. After excluding subjects without qualified genomic and neuroimaging (ASL and fMRI) data, 4,832 subjects from 17 research centers were finally included in this study.

Genotyping and imputation

Subjects were genotyped on the Illumina Infinium ASA-750K (Asian Screening Array). We excluded SNPs with a call rate <95% or minor allele frequency (MAF) < 0.001 and SNPs significantly deviated from Hardy-Weinberg equilibrium ($p < 1 \times 10^{-6}$). We excluded subjects with genotyping call rate <97%, excess heterozygosity (> mean ±5 standard deviations), or sex mismatch, and duplicated or related subjects (identity by decent >0.1875) with lower genotyping call rate. Principal component analysis (PCA) was used to evaluate genetic population substructure. Subjects with significant deviation from the population was removed and the top 10 principal components (PCs) were used as the covariate in the GWASs. After these quality control procedures, a total of 7,163 subjects and 549,309 variants (Figure S11) were included in imputation. Pre-phasing was performed using SHAPEIT[65] in chunks of 5000 kb with 250 kb overlap between chunks. Genotype imputation of autosomal SNPs was conducted with the IMPUTE2[66] with a merged panel of the 1000 Genomes Project (1KGP)[67] and the SG10K project.[68] After excluding variants with MAF <0.01 and information score (info) < 0.9, 6,830,145 autosomal SNPs were finally included in the GWASs.

Imaging data acquisition

All MRI data used in this study were acquired by three types of 3.0-Tesla MRI scanners (GE Discovery MR750, GE Discovery MR750w, and GE Signa HDxt). Foam padding was used to minimize head motion and earplugs were used to reduce scanner noise. All subjects were instructed to keep eyes closed, to move as little as possible, and to stay awake during scanning. The resting-state fMRI data were acquired using a gradient-echo single-short echo planar imaging sequence and were used to assess spontaneous neuronal activity; the resting-sate ASL data were acquired using a three-dimensional pseudo-continuous ASL sequence with a spiral fast spin-echo acquisition and were used to assess regional CBF; and the three-dimensional T1-weighted imaging (T1WI) data were acquired by a brain volume sequence and were used for estimating parameters for spatial normalization and calculating hippocampal volume. The specific MRI scanning parameters are provided Tables S14–S16.

Estimating parameters for spatial normalization

CAT12 (version r1364, http://dbm.neuro.uni-jena.de/cat) was used to preprocess T1WI images to estimate spatial normalization parameters. After the image inhomogeneity correction, we segmented the images into gray matter (GM), WM and CSF based on an adaptive Maximum A Posterior technique.[69] With SPM12 (http://www.fil.ion.ucl.ac.uk/spm), the Diffeomorphic Anatomical Registration Through Exponentiated Lie Algebra (DARTEL) algorithm[70] was applied to create the population-specific tissue probability templates for GM, WM, and CSF in the Montreal Neurological Institute (MNI) space based on the 5,743 CHIMGEN participants. The segmented T1WI images were spatially normalized to the population-specific templates using the DARTEL algorithm and were resampled into a cubic voxel of 1.5 mm. The estimated transformation parameters were also used for spatial normalization of fMRI and ASL images. Modulation was performed on the normalized GM images to preserve the absolute GM volume (GMV), from which we calculated the bilateral hippocampal volume defined by the AAL template.

CBF calculation

The ASL sequence can simultaneously generate the CBF, ASL, and proton density (PD) images. Since the signal to noise ratio (SNR) and contrast of CBF images were too low to perform skull stripping and spatial normalization, we generated the merged images to estimate the spatial normalization parameters of the CBF images. Based on the ASL images with good contrast but poor SNR and the PD images with good SNR but poor contrast, we merged the two sets of images to obtain a set of merged images with both high SNR and contrast using the following equation: merged images = (ASL images × PD images)/the mean value of all voxels in the ASL images. The merged images were just used to improve spatial normalization. Specifically, non-brain tissues in the merged images were stripped using the brain extraction tool. Individual skull-stripped images were aligned to the T1WI images using a boundary-based registration (BBR) function[71] and then were non-linearly normalized to the MNI space with the parameters estimated for T1WI images. Based on deformation parameter derived from the merged images, the CBF images of each subject were written into the MNI space and resampled to 3-mm isotropic voxels, and then spatially smoothed with a Gaussian kernel of 6-mm FWHM.

fMRI data preprocessing and metric calculation

The SPM12 was used to preprocess the fMRI data. The first 5 volumes of each subject were discarded to avoid unstable signals. The remaining volumes were corrected for the acquisition time delay between slices so that the collection times of all voxels were consistent within a repetition time. Then, we checked the head motion of each subject to ensure that it met the requirement (translation < 2mm and rotation < 2°) and realignment was performed to correct for head motion by rigid body transformation. The same method for the normalization of the CBF

images from the individual space to the MNI space was used to normalize fMRI images into the MNI space and the normalized images were resampled to 3-mm isotropic voxels. We calculated frame-wise displacement (FD) indexing volume-to-volume changes in head position. For each volume with FD > 0.5 mm, we defined this volume and one forward and two backward volumes as the imperfect volumes. We regressed out nuisance covariates including the average fMRI signals of WM (90% probability) and CSF (70% probability) defined by default masks in SPM12, 24 head motion parameters, imperfect volumes and linear trend of volumes. Finally, the fMRI data were band-pass filtered using a frequency range of 0.01 to 0.08 Hz. Since there are different signal sources in WM and CSF that cannot be reflected by the mean fMRI signals, we also used the CompCor approach[29] to estimate the first 10 principal components of the combined mask of WM and CSF, which were used to replace the mean fMRI signals of WM and CSF in the regression of nuisance covariates.

From the preprocessed fMRI data, we calculated three metrics (ReHo, ALFF, and fALFF) to assess spontaneous neuronal activity. ReHo was defined as the Kendall's coefficient of concordance (KCC) of the fMRI time series of this voxel with its nearest 26 voxels within the GM mask[72] ALFF was defined as the average square root of power spectrum in a low-frequency range (0.01–0.08 Hz),[73] and fALFF was the ratio of power spectrum of low-frequency to that of the entire frequency range to reduce the noise.[74] A 6-mm FWHM Gaussian kernel was used to smooth these maps. All preprocessing details are provided in Table S17.

Quality assessment for spatial normalization

Since distortion and signal wipeouts of the CBF and fMRI images may affect the quality of spatial normalization, we provided the following proof for proper preprocessing. First, we showed the T1WI, merged, and fMRI images (Figure S12) of a randomly selected subject to confirm that image quality was acceptable for spatial normalization. For this subject, we also showed successful co-registration of the merged and fMRI images with T1WI images (Figure S12). Second, we presented the segmented group-averaged GM images of 100 subjects and the 6th generation DARTEL template in MNI space (Figure S13), which indicates that segmentation and spatial normalization were successful. Third, we provided an overlay display of the group-averaged GM images with the bilateral hippocampal mask in MNI space (Figure S14), indicating good match in the hippocampi between the normalized images and the masks. Finally, we provided a parallel display for the group-averaged spatially normalized T1WI, CBF, and fMRI images (Figure S15) of the subjects, indicating satisfactory spatial normalization of CBF and fMRI images.

Calculation of hippocampal BOLD-CBF correlation

After reslicing the 1-mm^3 AAL mask[24] of the hippocampus into a 3-mm^3 hippocampal mask by the function of "reslice" in SPM12, we obtained a hippocampal mask of 552 voxels in MNI space. Before calculating hippocampal BOLD-CBF correlation, we used Combat[25] to harmonize the CBF, ReHo, ALFF and fALFF images that were calculated based on MRI data acquired by different scanners while adding age and sex as covariates to protect the variance of these two biological indicators. The harmonized CBF, ReHo, ALFF and fALFF images of each subject were normalized into *z*-scores to make them comparable across subjects. The hippocampal BOLD-CBF correlation was defined as the voxel-wise spatial correlation of ReHo, ALFF, and fALFF with CBF in this subject, which reflects the voxel-level consistency between spontaneous neuronal activity and blood flow in the hippocampus during rest. A rank-based inverse normal transformation was applied to these coupling measures. In this study, the ReHo-CBF correlation was used for discovery and the ALFF-CBF and fALFF-CBF correlations were used for robustness analyses. We also calculated ReHo-CBF correlation in each AAL region for the 4,832 participants. After removing WM and CSF signals with the CompCor approach,[29] we recalculated ReHo and hippocampal ReHo-CBF correlation. Pearson correlation was then used to test the consistency of hippocampal ReHo-CBF correlation calculated by the different approaches of nuisance regress. In eight participants with MRI data acquired at two different time points, we also calculated these coupling measures (ReHo-CBF, ALFF-CBF, and fALFF-CBF) and computed the intra-class correlation coefficient (ICC) of each measure. In the 4,832 subjects, we also tested the correlation of the ReHo-CBF correlation with the absolute and relative volumes for the bilateral hippocampi calculated by FreeSurfer v7.0 (https://surfer.nmr.mgh.harvard.edu/) using Pearson correlation.

Calculation of HRF shape parameters

To make comparison, we also calculated three shape parameters of the hemodynamic response function (HRF) including the response height (RH), time to peak (TTP), and full width at half maximum (FWHM) for 100 subjects randomly selected from the discovery sample. For each subject, the rsHRF toolbox[27] was used to calculate the three HRF shape parameters of each AAL region. We then calculated the Pearson correlation between ReHo-CBF correlation and HRF shape parameters in each brain region across the 100 subjects. Similarly, we also calculated and tested the correlation between ReHo-CBF correlation and HRF shape parameters in the bilateral hippocampal region.

QUANTIFICATION AND STATISTICAL ANALYSIS

Heritability of hippocampal BOLD-CBF correlation

Based on the 6,830,145 autosomal SNPs, we estimated the SNP heritability of the hippocampal BOLD-CBF correlation in 4,832 subjects with the GREML-LDMS method.[28] The covariates used in the SNP heritability estimation were the same as those used in the GWAS, including the age, sex, $age,^2$ age × sex, age^2 × sex, first ten PCs, and FD. The SNP heritability estimation was conducted for the hippocampal BOLD-CBF correlation measures derived from all five approaches.

GWAS design and statistical methods

For the 6,830,145 autosomal SNPs, a two-stage GWAS was designed to explore genetic associations of the hippocampal ReHo-CBF correlation. The discovery and replication samples included 4,606 and 426 subjects, respectively. In each GWAS, linear regression with an additive model was conducted to investigate the association between the dosage of each variant and each imaging phenotype by Plink2[60] with age, sex, age,^{2} age × sex, age^2 × sex, first ten PCs, and FD as covariates. In the discovery stage, genome-wide significance was defined as $p < 5 \times 10^{-8}$. In the replication stage, we replicated each genome-wide significant SNP identified in the discovery stage with a threshold of $p < 0.05$. Finally, we combined the GWAS results of the two samples by fixed-effects inverse-variance weighted meta-analysis using METAL.[61] In this study, significant SNPs were defined as those met the following two criteria: $p < 5 \times 10^{-8}$ in the discovery sample and $p < 0.05$ in the replication sample with the same direction of the effect. Details about genetic associations were presented using regional plots generated by LocusZoom.[62] We compared GWAS results on ReHo-CBF correlation with previous GWASs on the bilateral hippocampal volume[30,31] to find overlapping SNP, which was in the same position and had the same alleles, meanwhile was significant in both GWASs ($p < 5 \times 10^{-8}$) because of the difference LD structure among different ancestry.

Robustness analyses by variation of the NVC phenotype

Four robustness analyses were conducted to confirm the identified genome-wide significant associations for hippocampal BOLD-CBF correlation assessed by the ReHo-CBF correlation. Since we don't know which fMRI measure is the best indicator for regional spontaneous neuronal activity, we also used other two fMRI measures (ALFF and fALFF) to reflect regional spontaneous neuronal activity and calculated ALFF-CBF and fALFF-CBF correlations to represent hippocampal BOLD-CBF correlation and re-performed GWASs to verify the main results. Since the spatial range of the hippocampus is slightly varied in different brain atlases, we also extracted the hippocampal voxels based on another atlas (BNA)[26] and recalculated hippocampal ReHo-CBF correlation and re-performed GWASs. Since the GSR during preprocessing is matter of debate in the field of resting-state fMRI data analyses,[75] we also regressed out global signals during fMRI data preprocessing and recalculate ReHo and ReHo-CBF correlations and re-performed GWASs. Based on the hippocampal ReHo-CBF correlation calculated from fMRI data preprocessed by the CompCor approach,[29] we re-performed GWAS in the 4,832 participants. In addition, we also conducted GWAS for the ReHo-CBF correlation of the bilateral precentral gyri in the 4,832 participants.

Single- and multi-trait GWASs

In the 4,832 subjects, we also conducted GWAS for the hippocampal mean CBF and mean ReHo, respectively. Moreover, we used three multivariate methods (MTAG,[32] CGWAS and MinGWAS[33]) to conduct genetic association analyses by integrating the three phenotypes (ReHo, CBF, and ReHo-CBF correlation). The significance threshold and covariates were the same as the GWAS for ReHo-CBF correlation.

Functional annotations

To characterize variants' functions, significant SNPs were annotated by Variant Effect Predictor (https://www.ensembl.org/info/docs/tools/vep/index.html) and ANNOVAR.[63] HaploReg v4[76] and RegulomeDB[77] were used to assess chromatin state and functional motifs of variants in LD ($r^2 \geq 0.8$ in EAS of 1KGP3) with the lead SNPs. We also searched the roles of the identified significant SNPs as expression quantitative trait loci from the QTLbase[78] and checked their relations with brain gene expression in the Braineac database (http://www.braineac.org/).

Gene-based association analysis and enrichment analyses

Translation of the genome-wide association signals of SNPs into genes contributes to the identification of biological pathways and functional mechanisms of complex human traits. Therefore, we conducted gene-based association analysis based on the meta-analysis results by the MAGMA 1.09.[64] We assigned genetic variants to protein-coding genes based on their positions according to the NCBI 37.3 (hg19) build. After excluding SNPs in the major histocompatibility complex (MHC), 18,000 genes containing at least one qualified genetic variant were included gene-based association analysis. The multiple testing was adjusted for the number of genes (n = 18,000) with a Bonferroni corrected threshold of $p = 2.78 \times 10^{-6}$. And we also performed robustness analyses with additional four hippocampal BOLD-CBF phenotypes to confirm the main results. Next, all the 18000 genes for the gene-based association analysis were included in tissue-specific and cell-specific enrichment analyses. In tissue-specific enrichment analysis, gene expression profiles of 54 different types of tissues were derived from GTEx v8.[79] The cell-specific enrichment analysis was conducted based on the gene expression data of 39 cell types.[80,81] Pathway enrichment involved in 10,226 pathways derived from the KEGG, REACTOME, BIOCARTA and GO Terms pathway-gene data (downloaded via the Molecular Signatures Database 7.4, http://www.gsea-msigdb.org/gsea). These enrichment analyses also conducted for four additional hippocampal BOLD-CBF correlations to test the reliability of these results.